Research Square

Preprints are preliminary reports that have not undergone peer review.
They should not be considered conclusive, used to inform clinical practice,
or referenced by the media as validated information.

Finite Element Analysis of Femoral Neck System Versus Parallel and Non-Parallel Cannulated Screw Configurations in Pauwels Type III Femoral Neck Fractures

Amit Kumar

amit2k03@gmail.com

Sanjay Gandhi Post Graduate Institute of Medical Sciences

Ajeet Kumar

Indian Institute of Technology Delhi

Somesh Gupta

Indian Institute of Technology Delhi

Alok Rai

Institute of Medical Sciences

Research Article

Keywords: Fracture neck of femur, Fracture fixation, Bone Screws, Finite element analysis, Biomechanical Phenomena, Femoral Neck system

Posted Date: May 26th, 2026

DOI: https://doi.org/10.21203/rs.3.rs-9771684/v1

License: This work is licensed under a Creative Commons Attribution 4.0 International License. Read Full License

Additional Declarations: No competing interests reported.

Abstract

Introduction: The Femoral Neck System has been suggested for fixation of fracture neck of femur, with the advantages of controlled dynamic axial compression, low invasiveness, and angular stability. Its biomechanical advantage over non-parallel CCS configurations for Pauwels type III fractures has been the subject of recent biomechanical analyses.

Objective: The study explored the biomechanical performance of parallel & non-parallel configurations of CCS and FNS for Pauwels type III FNF using finite element analysis by examining the displacement and stress of the bone and the internal fixation device.

Methods: DICOM format images of saw bone was used to build the 3-D geometric models which were hyper meshed to create models of Pauwels type III FNF with angle of 65°. CAD models of four configurations were created as per AO specification and analysed for stress distribution of bone & implant, relative displacement between fracture planes & stiffness.

Results: Superior stability was demonstrated by the 4-CCS configuration, which exhibited the lowest stress at the fracture surface, minimal implant stress, smallest inter-fragmentary displacement, and highest construct stiffness. Additionally, BDSF outperformed 3-CCS and FNS in terms of biomechanical performance. Compared to non-parallel CCS configurations, FNS showed higher implant stress at the bolt-anti-rotation screw junction, higher stress concentrations in the sub-trochanteric area, and higher fracture gap displacement, indicating a higher likelihood of mechanical failure and sub-trochanteric fracture.

Conclusion: The non-parallel configuration of BDSF and 4-CCS demonstrated improved biomechanical features over FNS. While 4-CCS provided the highest stability, BDSF may offer a more clinically feasible alternative. These findings should be interpreted in the context of finite element assumptions, and further clinical studies are required to validate their translational relevance.

Introduction

Orthopaedic surgeons continue to face difficulties with fractures of the neck of the femur (FNF), sometimes known as "the unsolved fracture" [1]. Regardless of fracture morphology, several biomechanical studies have suggested a stable fixation to prevent complications such as non-union, neck shortening, implant back-out, varus collapse, and avascular necrosis [2]. In Pauwels type III fractures, high shear and bending forces contribute to increased rates of fixation failure, non-union, and femoral head necrosis [3, 4]. Conventional parallel CCS fixation provides limited resistance to these forces and may result in neck shortening and implant protrusion due to uncontrolled dynamic compression [5].

To improve stability, non-parallel screw configurations such as 4-CCS (Alpha configuration) and BDSF have been proposed with encouraging clinical outcomes [6–11]. More recently, the Femoral Neck System (FNS) has been introduced as a minimally invasive fixation device providing angular stability with controlled dynamic compression [12–14]. Previous studies have demonstrated superior biomechanical and clinical performance of FNS compared with conventional 3-CCS fixation [15–17]. However, its biomechanical advantage over non-parallel configurations of CCS for Pauwels type III fractures has been the subject of investigation among

biomechanical analyses. The purpose of this study is to compare the biomechanical properties of different CCS configurations with FNS using Finite Element Analysis for Pauwels type III FNFs.

Material & Methods

The study was registered in the Institute Research Cell (IITD/DPGSR/MSR-468). As this study expands on our previously published finite element analysis, its scope is significantly different due to the inclusion of the Femoral Neck System [18].

A CT scanner was used to scan the whole length of the femur saw bone. The 3-D geometric model of the femur was then exported in STL format after the data in DICOM format was moved to the program MIMICS. Hyper Mesh software (version 2019) was used to import the femur's STL files.1) to form a fracture with a 65º angle and smooth the surface mesh [Figure 1A]. Boolean approaches were used to combine the implant elements and the geometric model of the bone using SolidWorks software. For additional simulation, the constructed 3-D meshed models of the fixing technique were imported into Abaqus.

Four fixation constructs [Figure1B] were modelled based on standard surgical configurations: (i) three parallel cannulated compression screws arranged in an inverted triangular configuration[19]; (ii) biplanar double-supported fixation with divergent screw orientation providing calcar support [20]; (iii) four cannulated compression screws in an alpha configuration with an additional off-axis screw[21] and (iv) the Femoral Neck System, consisting of a bolt, anti-rotation screw, and distal locking screw connected via a side plate[12]. Based on previous study, SolidWorks software was used to create all cannulated screws with a diameter of 7.3mm and a thread length of 16mm, maintaining a 5mm subchondral distance from the femoral head[22].

The threaded portion of the screw was simplified by modelling it as smooth surfaces with diameters that matched the intended thread size and length because the thread was not the focus of this investigation

Table 1
Material properties of implants and bones with interfacial conditions between different components according to Li J et al[22]

Material	**Young' s Modulus (MPa)**	**Poisson' Ratio**	**Tensile Strength (MPa)**
Cortical Bone	17000	0.3	106
Cancellous Bone	155	0.3	6
Stainless steel	200000	0.3	766
Titanium	110000	0.30	950
Interface	**Condition**		
Implant-Bone	Frictional Contact (μ = 0.3)		
Between fracture planes	Frictional contact (μ = 0.46)		
Cortical bone-Cancellous bone	Fully Bonded		
Threaded part of screws-Bone	Fully Bonded		

Synthetic bone and implants were assumed to be of homogeneous, isotropic, and linearly elastic properties. All the implants' properties were made of titanium alloy and stainless steel[Table 1]. Based on previous studies[22], the bone–implant and fracture interfaces were modelled as frictional contacts with coefficients of friction of 0.30 and 0.46 respectively[Table 1]. A tie constraint was applied between the threaded screw portion and femoral head to prevent relative motion. Increased friction along the smooth screw shaft optimized resistance to implant–bone motion. This differential bonding conditions enabled independent assessment of fixation mechanics at the fracture site.

Boundary and loading conditions

A hip reaction force of 2100N, representing approximately three times the body weight of a 70-kg individual, was applied to the load-bearing region of the femoral head. To simulate single-leg stance, the load was oriented at 10° abduction and 9° posterior inclination[22]. A preload of 224N was applied along the implant axis to simulate fracture compression. All nodes at the distal femur were fully constrained to prevent rigid body motion during simulation[23].

Validation of our model

To validate the models, we used 3-CCS configuration and compared our findings [Table 2] with three existing 3-CCS literatures. After providing the identical properties, models by Li et al.[22], Huang et al.[23], Zhan et al.[24], and our model showed comparable value trends. Our models and the models by Li et al.[22] showed a comparable distribution pattern on the nephogram[figure1C/1D]. Thus, our model was validated for future research.

Table 2
Comparison of our model results with the works of literature for Validation of models

S.no	Parameter	Our model	Literature[22]	Our model	Literature[23]	Our model	Literature[24]
1.	**MSI**	**328.8**	**363.43**	**319.1**	**336.3**	**216.2**	**196.04**
2.	MSB	105.1	116.32	156.2	138.8	93.68	
3.	MDI	3.086	7.9592	4.537	1.262	2.492	2.893
4.	MDB	3.502	8.1479	5.73	1.342	2.697	3.149

Outcome Measures:

In the finite element analysis, displacement was evaluated in the bone, implant, and across the fracture interface, while stress distribution was assessed in the bone, fracture surface, and implant. Construct stiffness was calculated as a measure of overall model stability. These biomechanical parameters were compared between the FNS and various CCS configurations.

Result

Von Mises Stress Distribution in Femur Bone

Stress distribution was analysed to identify regions susceptible to mechanical failure. In titanium models, the maximum stress in bone (MSB) was 90.64MPa in the 3-CCS and 79.69MPa in the BDSF (Figure2A). In both constructs, peak stress was concentrated in the calcar region along the fracture line.

In the 4-CCS configuration, the maximum stress was 95.45MPa and was localized at the interface between the off-axis screw and the lateral cortex, indicating redistribution of stress away from the fracture site.

The FNS model demonstrated the highest overall bone stress(128.7MPa), predominantly located in the subtrochanteric region at the distal screw–bone junction, suggesting an increased risk of subtrochanteric fracture.

A similar trend was observed in stainless-steel models, with MSB values of 74.64MPa, 59.90MPa, 89.84MPa, and 127.2MPa for 3-CCS, BDSF, 4-CCS, and FNS configurations, respectively.

Maximum Stress at Fracture Surface (MSFS)

Excessive stress at the fracture interface may increase micromotion and impair fracture healing. In all configurations, the highest stress at the fracture surface was consistently observed in the inferior region of the fracture plane(Figure2B).

The 4-CCS configuration demonstrated the lowest MSFS, indicating a more favourable biomechanical environment for fracture healing. The addition of an off-axis screw reduced MSFS from 87.19MPa in the 3-CCS model to 60.92MPa in the 4-CCS model, representing an approximate 30% reduction.

The BDSF configuration also demonstrated reduced MSFS (79.69MPa), reflecting improved load distribution across the fracture interface. In contrast, the FNS model exhibited an MSFS of 84.97MPa, which remained higher than both BDSF and 4-CCS configurations, indicating comparatively inferior stress distribution at the fracture site.

A comparable trend was observed in stainless-steel models, with MSFS values of 71.83MPa, 54.83MPa, 51.70MPa, and 71.91MPa for 3-CCS, BDSF, 4-CCS, and FNS configurations, respectively.

Von Mises stress distribution of implant

Stress distribution within the implant was analysed to identify regions susceptible to mechanical failure under loading conditions. In titanium models, the maximum stress in the implant (MSI) was 322.5MPa in the 3-CCS configuration, 262.8MPa in the BDSF configuration, and 153.6MPa in the 4-CCS configuration, approximately 52% less than 3-CCS. In all CCS constructs, peak stress was consistently localized at the central portion of the inferior screw, identifying it as the primary load-bearing component.

In contrast, the FNS model demonstrated the highest MSI(441MPa), concentrated at the junction between the bolt and anti-rotation screw (Figure 2C), indicating a potential structural stress concentration point within the construct.

A similar trend was observed in stainless-steel models, with MSI values of 332.9MPa, 298.7MPa, 184.6MPa, and 502.9MPa for 3-CCS, BDSF, 4-CCS, and FNS configurations, respectively.

Overall, the 4-CCS configuration demonstrated the lowest MSI among all models, suggesting a lower risk of implant deformation or mechanical failure.

Displacement Distribution in Bone and Implant

Displacement was evaluated as an indicator of construct stability. Maximum displacement in bone(MDB) was consistently observed at the apex of the femoral head across all configurations(Figure 3A). Similarly, maximum displacement in the implant(MDI) occurred at the terminal portions of the fixation devices(Figure 3B). In the FNS model, peak implant displacement was localized at the tip of the anti-rotation screw, whereas in CCS configurations it was concentrated at the tip of the superior–posterior screw.

Quantitative analysis (Table 3) demonstrated that the 3-CCS configuration exhibited the highest displacement values in both bone and implant, indicating the lowest construct stability. In contrast, the 4-CCS configuration demonstrated the least displacement, reflecting superior resistance to deformation under load.

Compared with the BDSF and 4-CCS configurations, the FNS model demonstrated greater displacement in both bone and implant, suggesting comparatively inferior mechanical stability in vertically oriented fracture patterns.

S. No.	Parameter (Unit)	3-CCS (Ti)	3-CCS (SS)	BDSF (Ti)	BDSF (SS)	4-CCS (Ti)	4-CCS (SS)	FNS (Ti)	FNS (SS)
1	MSB (MPa)	90.64	74.64	79.69	59.90	95.45	89.84	128.7	127.2
2	MSFS (MPa)	87.19	71.83	79.69	54.83	60.92	51.70	84.97	71.91
3	MSI (MPa)	322.5	332.9	262.8	298.7	153.6	184.6	441	502.9
4	MDB (mm)	3.427	2.833	2.618	2.275	2.09	1.923	2.769	2.466
5	MDI (mm)	3.100	2.57	2.288	1.999	1.898	1.750	2.321	2.054
6	MIFD (mm)	1.006	0.653	0.637	0.452	0.35	0.259	0.659	0.503
7	Stiffness (N/mm)	2087.47	3215.92	3296.70	4646.01	6000	8108.10	3186.64	4174.55

Table 3: Comparative Biomechanical Parameters Across Various Configurations under simulated environment in the study

Maximum Interfragmentary Displacement at Fracture Gap (MIFD)

Interfragmentary displacement is an important determinant of fracture healing. In the present study, displacement across the fracture gap was calculated by measuring the relative motion between corresponding nodes on opposing fracture surfaces(Figure 3C).

In titanium models, MIFD was 1.006mm for 3-CCS, 0.637mm for BDSF, 0.35mm for 4-CCS, and 0.659mm for FNS. A similar trend was observed in stainless-steel models, with corresponding values of 0.653mm, 0.452mm, 0.259mm, and 0.503mm, respectively (Table3).

Among all configurations, the 4-CCS construct, particularly with stainless-steel implants, demonstrated the lowest MIFD, indicating superior mechanical stability and a more favourable environment for fracture healing. In contrast, the 3-CCS and FNS configurations exhibited comparatively higher MIFD, suggesting reduced stability and a potential risk of delayed union or non-union.

Notably, the FNS model demonstrated greater MIFD than both BDSF and 4-CCS configurations, indicating inferior control of interfragmentary motion in vertically oriented fracture patterns.

Stiffness calculations

Construct stiffness was calculated as the ratio of applied load to MIFD and used as a direct measure of mechanical stability.

In titanium models, stiffness values were 2087.47N/mm for 3-CCS, 3296.70N/mm for BDSF, 6000N/mm for 4-CCS, and 3186.64N/mm for FNS. A similar trend was observed in stainless-steel models, with corresponding values of 3215.92N/mm, 4646.01N/mm, 8108.10N/mm, and 4174.55N/mm, respectively.

Statistical analysis

Statistical analyses were performed for exploratory purposes to characterize relationships within the simulated dataset. These analyses are descriptive and should not be interpreted as predictive of clinical outcomes.

Pearson correlation analysis (Table 4A, Figure 4A) demonstrated a strong negative correlation between construct stiffness and displacement parameters (MDB and MIFD; r = −0.91), indicating that increased stiffness was associated with reduced motion at the bone and fracture interface. A near-perfect positive correlation was observed between MDB and MIFD (r = 0.99), suggesting that overall bone displacement closely parallels interfragmentary motion. A moderate negative correlation was found between stiffness and implant stress (MSI; r = −0.58), indicating that stiffer constructs may distribute implant stress more effectively. In contrast, MSB demonstrated minimal correlation with stiffness (r = −0.08), suggesting that bone stress is influenced more by implant design than by construct rigidity alone. Regression analysis (Figure 4B) demonstrated a strong inverse linear relationship between construct stiffness and interfragmentary displacement, described by the equation:

MIFD =1.0369-(0.0001088 x Stiffness)

The regression model showed good explanatory power (R^2 = 0.82), indicating that approximately 82% of the variation in fracture-gap displacement could be explained by construct stiffness. For every 1000 N/mm increase in stiffness, MIFD decreased by approximately 0.11 mm.

We could estimate the stiffness required to reach clinical stability thresholds [Table 4B]. The analysis[figure 4B] confirms that the 4-CCS(SS) is the only construct in the data that reliably achieves a displacement level below 0.26mm. To push stability even further (e.g., below 0.2mm), a construct would need a stiffness exceeding 7,700 N/mm, which the 4-CCS(SS) already accomplished (8108.10N/mm).

We calculated the Percentage Increase in Stability [Table 4C, Figure 4C], using Stiffness as the primary indicator and MIFD as the secondary indicator with 3-CCS(Ti) construct, as baseline with the least stable configuration. Among all configurations, the 4-CCS model demonstrated the highest stiffness, particularly with stainless-steel implants, indicating superior resistance to deformation under load. In contrast, the 3-CCS configuration exhibited the lowest stiffness, reflecting reduced structural stability. The FNS model showed intermediate stiffness values but remained inferior to both BDSF and 4-CCS configurations. The overall higher stiffness observed in stainless-steel models can be attributed to their greater Young's modulus compared to titanium, resulting in increased resistance to elastic deformation[25].

Parameter	Stiffness	MDB	MIFD	MSB	MSI
Stiffness	(1.00)	(-0.91)	(-0.91)	(-0.08)	(-0.58)
MDB	(-0.91)	(1.00)	(0.99)	(0.08)	(0.46)
MIFD	(-0.91)	(0.99)	(1.00)	(0.05)	(0.41)
MSB	(-0.08)	(0.08)	(0.05)	(1.00)	(0.59)
MSI	(-0.58)	(0.46)	(0.41)	(0.59)	(1.00)

(a)

Target MIFD (mm)	Predicted Stiffness Required (N/mm)	Matching Construct
0.50 mm	~4,936 N/mm	Close to BDSF (SS)
0.35 mm	~6,314 N/mm	Close to 4-CCS (Ti)
0.20 mm	~7,693 N/mm	Surpassed by 4-CCS (SS)

(b)

Rank	Construct	Stiffness (N/mm)	Stability Increase (%)	MIFD (mm)	Displacement Reduction (%)
1	4-CCS (SS)	8108.10	+288.4%	0.259	-74.3%
2	4-CCS (Ti)	6000.00	+187.4%	0.350	-65.2%
3	BDSF (SS)	4646.01	+122.6%	0.452	-55.1%
4	FNS (SS)	4174.55	+100.0%	0.503	-50.0%
5	BDSF (Ti)	3296.70	+57.9%	0.637	-36.7%
6	3-CCS (SS)	3215.92	+54.1%	0.653	-35.1%
7	FNS (Ti)	3186.64	+52.7%	0.659	-34.5%
8	3-CCS (Ti)	2087.47	*Baseline*	1.006	*Baseline*

(c)

Table 4 (a): Pearson Correlation Matrix of Biomechanical Parameters. The correlation coefficients (r) between the key mechanical parameters. Values closer to (1) or (-1) indicate a stronger relationship; (b): Predicted Structural Requirements for Clinical Stability Targets. This table utilizes the linear regression model MIFD =1.0369-(0.0001088 x Stiffness) to identify the specific mechanical thresholds needed to achieve various levels of interfragmentary stability; (c): Construct Stability Ranking with Percentage Increase in stability and displacement reduction

Discussion

Femoral Neck System has been introduced as a minimally invasive fixation device that combines angular stability with controlled dynamic compression[12–14]. Biomechanical studies have demonstrated its stability, comparable to DHS and superior to conventional parallel 3-CCS fixation[15–17]. However, its biomechanical advantage over non-parallel CCS configurations for Pauwels type III fractures has been the subject of investigation among biomechanical analyses.

Our study demonstrated distinct variations in biomechanical properties between FNS And CCS configurations. In the 3-CCS and BDSF models, peak stress was localized in the calcar region along the fracture line, whereas in the 4-CCS configuration, the highest stress was observed at the interface between the off-axis screw and the lateral cortex. This indicates that the addition of an off-axis screw in the 4-CCS construct shifts stress concentration away from the fracture site toward the lateral cortex, thereby reducing mechanical loading at the fracture interface. In contrast, the concentration of high stress near the fracture site in the 3-CCS configuration may increase local mechanical load and adversely affect fracture healing. These findings are consistent with previous studies by Xia et al [26]., Ma et al. [27], and Li et al. [28], which also reported lower stress at the fracture site and subtrochanteric region in non-parallel screw configurations compared to fixed-angle devices such as FNS. Conversely, the elevated stress observed in the subtrochanteric region in the FNS model may indicate a higher risk of stress-related complications, including subtrochanteric fracture, as described in prior clinical study [29]. The relative risk of subtrochanteric fracture appears to decrease in the order of FNS, 4-CCS, BDSF, and 3-CCS, which may be attributed to the progressively reduced implant footprint and more favourable stress distribution patterns in these configurations.[30]

In both 3-CCS and 4-CCS configurations, peak implant stress was localized at the central region of the inferior screw, identifying it as the principal load-bearing component. In contrast, the BDSF configuration exhibited maximum stress in the posterior–inferior screw, suggesting a redistribution of load among the screws, with this screw bearing the highest mechanical demand and thus being more susceptible to bending deformation. Notably, the addition of an off-axis screw in the 4-CCS configuration resulted in a substantial reduction in implant stress, with approximately 52% decrease in MSI compared to the 3-CCS model. This finding reflects improved load distribution and reduced stress concentration within the construct. In the FNS model, peak implant stress was concentrated at the junction between the bolt and anti-rotation screw. This localized stress concentration may be attributed to the structural design of the device, particularly the interface between these components, which can act as a stress riser [28]. Consequently, the FNS configuration demonstrated the highest implant stress among all models, indicating a potential risk of mechanical failure. These findings are consistent with previous finite element studies, which have reported higher implant stress in fixed-angle devices such as FNS compared to non-parallel cannulated screw configurations. Overall, the titanium 4-CCS model, exhibiting the lowest implant stress, appears to offer the least risk of implant deformation among the evaluated configurations [25].

Displacement was evaluated at both the bone and implant levels, as well as across the fracture gap by measuring relative motion between corresponding nodes on opposing fracture surfaces. Consistent with previous studies [22–24, 26–28], the 3-CCS configuration exhibited the highest displacement, indicating inadequate resistance to shear forces in Pauwels type III fractures. In contrast, both BDSF and 4-CCS configurations demonstrated significantly lower displacement in bone, implant, and fracture gap, reflecting

improved mechanical stability. These findings suggest that non-parallel screw configurations provide more effective control of interfragmentary motion under high shear conditions. The FNS model demonstrated greater displacement compared to BDSF and 4-CCS configurations, indicating comparatively inferior stability. This observation is in agreement with previous finite element studies [26–28], which have reported higher displacement and reduced stability in fixed-angle constructs when used for vertically oriented femoral neck fractures.

From clinical perspective, achieving rigid fixation is essential in Pauwels type III femoral neck fractures to counteract high shear and rotational forces and to facilitate early postoperative mobilization, thereby reducing the risk of complications. In the present study, the 4-CCS configuration demonstrated the highest construct stiffness among all models, indicating superior resistance to deformation under load. In contrast, the FNS configuration exhibited comparatively lower stiffness than non-parallel cannulated screw constructs, suggesting reduced mechanical stability in Pauwels type III fracture. These findings are consistent with previous biomechanical studies, including those by Xia et al. [26], which have reported inferior performance of FNS compared to non-parallel screw configurations in managing high-shear femoral neck fractures.

Limitation

This study has limitations inherent to finite element modelling. The use of a synthetic femur with homogeneous, isotropic, and linearly elastic properties does not fully represent the anisotropic and viscoelastic nature of human bone, limiting generalizability, particularly to osteoporotic populations. The fracture was idealized as a uniform Pauwels type III pattern (65°), without accounting for patient-specific anatomical variation. Loading conditions simulated static single-leg stance and did not include dynamic forces such as gait or muscle loading. The screw–bone interface was simplified using frictional and bonded contacts, with threads modelled as smooth surfaces, which may not accurately reflect micromotion or loosening. Additionally, the analysis assessed only initial mechanical stability and did not incorporate biological factors such as fracture healing, remodelling, or vascularity. Cyclic loading and long-term fatigue behaviour were not evaluated, and surgical feasibility, including implant crowding and vascular risk, was not considered.

Conclusion

Contrary to its proposed advantages, FNS demonstrated comparatively lower biomechanical stability under simulated conditions of Pauwels type III fractures. The performance of FNS may be attributed to its fixed-angle design, which behaves as a load-bearing construct rather than a load-sharing system. Despite its biomechanical superiority, the 4-CCS configuration may not always be practically achievable, and alternative constructs such as BDSF may offer a more balanced combination of biomechanical stability and surgical feasibility. However, further clinical studies are required to validate these biomechanical observations and determine their translational relevance in patient outcomes.

Abbreviations

MSB
Maximum Stress in Bone
MSFS

Maximum Stress at Fracture Surface
MSI
Maximum Stress in Implant
MDB
Maximum Displacement in Bone
MDI
Maximum Displacement in Implant
MIFD
Maximum Interfragmentary Displacement
Ti
Titanium
SS
Stainless Steel
CCS
Cannulated Compression Screws
BDSF
Biplanar Double–Supported Fixation
FNS
Femoral Neck System

Declarations

Declarations of interest: none

Human Ethics and Consent to Participate declarations: not applicable.

Author Contribution

A K : Conceptualization, Writing- Original draft preparation;Aj K: Project administration; Resources; Software; Supervision; Validation;S K: Data curation; Formal analysis;AR: Writing - review & editing

Acknowledgement

I wish to acknowledge my alma-mater IMS, BHU for teaching basic knowledge of orthopaedic & thanks my family for constant support.

Data Availability

“The data supporting the findings of this study, including finite element models and simulation outputs, are available from the corresponding author upon reasonable request.”

References

1. Fracture neck of (2016) femur - Still an unsolved issue. J Orthop 13(1):A1–3
2. Augat P, Bliven E, Hackl S (2019) Biomechanics of femoral neck fractures and implications for fixation. J Orthop Trauma 33(Suppl 1):S27–S32
3. Cha YH, Yoo JI, Hwang SY, Kim KJ, Kim HY, Choy WS et al (2019) Biomechanical evaluation of internal fixation of Pauwels type III femoral neck fractures: A systematic review of various fixation methods. Clin Orthop Surg 11(1):1–14
4. Parker MJ (2009) Results of internal fixation of Pauwels type-3 vertical femoral neck fractures. J Bone Joint Surg Am 91(2):490–491
5. Felton J, Slobogean GP, Jackson SS, Della Rocca GJ, Liew S, Haverlag R et al (2019) Femoral neck shortening after hip fracture fixation is associated with inferior hip function: results from the FAITH Trial. J Orthop Trauma 33(10):487–496
6. Sami A, Prabhakar R, Kumar Yadav A, Kumar Jain V (2022) Biplane double supported screw fixation for femoral neck fracture in young adults: A prospective cohort study. J Orthop 33:117–123
7. Jiang D, Zhan S, Cai Q, Hu H, Jia W (2021) Long-term differences in clinical prognosis between crossed- and parallel-cannulated screw fixation in vertical femoral neck fractures of non-geriatric patients. Injury 52(11):3408–3414
8. Gumustas SA, Tosun HB, Agır I, Orak MM, Onay T, Okcu G (2014) Influence of number and orientation of screws on stability in the internal fixation of unstable femoral neck fractures. Acta Orthop Traumatol Turc 48(6):673–678
9. Galal S, Nagy M (2017) Non-parallel screw fixation for femoral neck fractures in young adults. J Clin Orthop Trauma 8(3):220–224
10. Filipov O, Stoffel K, Gueorguiev B, Sommer C (2017) Femoral neck fracture osteosynthesis by the biplane double-supported screw fixation method (BDSF) reduces the risk of fixation failure: clinical outcomes in 207 patients. Arch Orthop Trauma Surg 137(6):779–788
11. Forsh DA, Ferguson TA (2012) Contemporary management of femoral neck fractures: the young and the old. Curr Rev Musculoskelet Med 5(3):214–221
12. Stoffel K, Zderic I, Gras F, Sommer C, Eberli U, Mueller D, Oswald M, Gueorguiev B (2017) Bio mechanical evaluation of the femoral neck system in unstable Pauwels III femoral neck fractures: a comparison with the dynamic hip screw and cannulated screws. J Orthop Trau ma 31:131–137
13. Schopper C, Zderic I, Menze J, Muller D, Rocci M, Knobe M et al (2020) Higher stability and more predictive fixation with the femoral neck system versus Hansson pins in femoral neck fractures Pauwels II. J Orthop Translat 24:88–95
14. Jung CH, Cha Y, Yoon HS, Park CH, Yoo JI, Kim JT, Jeon Y (2022) Mechanical effects of surgical variations in the femoral neck system on Pauwels type III femoral neck fracture: a finite element analysis. Bone Joint Res 11:102111
15. Hu H, Cheng J, Feng M et al (2021) Clinical outcome of femoral neck system versus cannulated compression screws for fixation of femoral neck fracture in younger patients. J Orthop Surg Res 16:370
16. Jiang T, Gao H, Xu B, Lv F, Liu T The comparison of femoral neck system and cancellous screws internal fixation for femoral neck fracture. Biotechnol Genet Eng Rev 1–12

17. He C, Lu Y, Wang Q, Ren C, Li M, Yang M, Xu Y, Li Z, Zhang K, Ma T Comparison of the clinical efficacy of a femoral neck system ver sus cannulated screws in the treatment of femoral neck fracture in young adults
18. Kumar A, Kumar S, Kumar A, Keshav K, Baghel A, Sharma P (2025) Finite element analysis of sliding vs static configuration of partial threaded cannulated compression screws for Pauwels type III fracture neck of femur. J Clin Orthop Trauma 66:103024
19. Forsh DA, Ferguson TA (2012) Contemporary management of femoral neck fractures: the young and the old. Curr Rev Musculoskelet Med 5(3):214–221
20. Filipov O, Gueorguiev B (2015) Unique stability of femoral neck fractures treated with the novel biplane double-supported screw fixation method: a biomechanical cadaver study. Injury 46(2):218–226
21. Jiang D, Zhan S, Cai Q, Hu H, Jia W (2021) Enhanced interfragmentary stability and improved clinical prognosis with use of the off-axis screw technique to treat vertical femoral neck fractures in nongeriatric patients. J Orthop Surg Res 16(1):473
22. Li J, Zhao Z, Yin P, Zhang L, Tang P (2019) Comparison of three different internal fixation implants in treatment of femoral neck fracture-a finite element analysis [published correction appears in. J Orthop Surg Res 14(1):106
23. Huang S, Zhang Y, Zhang X, Zhou C, Li W, Wang Y et al (2023) Comparison of femoral neck system and three cannulated cancellous screws in the treatment of vertical femoral neck fractures: clinical observation and finite element analysis. Biomed Eng Online 22(1):20
24. Zhan S, Jiang D, Xu J, Ling M, Yang K, Li Y et al (2020) Influence of the proximal screws of buttress plates on the stability of vertical femoral neck fractures: a finite element analysis. BMC Musculoskelet Disord 21(1):842
25. Barber CC, Burnham M, Ojameruaye O, McKee MD (2021) A systematic review of the use of titanium versus stainless steel implants for fracture fixation. OTA Int 4(3):e138
26. Xia Y, Zhang W, Hu H, Yan L, Zhan S, Wang J (2021) Biomechanical study of two alternative methods for the treatment of vertical femoral neck fractures - A finite element analysis. Comput Methods Programs Biomed 211:106409
27. Ma J, Zhao Z, Zhi X et al (2022) Finite element comparative analysis of three different internal fixation methods in the treatment of Pauwels type III femoral neck fractures. BMC Musculoskelet Disord 23:1030
28. Li N, Cheng KY, Fan J et al (2024) Evaluating three internal fixation techniques for Pauwels III femoral neck fractures via finite element analysis. Sci Rep 14:15519
29. Fisher JC, Gerzina C, Rush K et al (2023) Subtrochanteric fracture after femoral neck system of femoral neck fractures: a report of four cases. BMC Musculoskelet Disord 24:749
30. Hsu MR, Shu HT, Luksameearunothai K, Margalit A, Yu AT, Hasenboehler EA, Shafiq B (2022) Is there an increased risk for subtrochanteric stress fracture with the Femoral Neck System versus multiple cannulated screws fixation? J Orthop 30:127–133

Figures

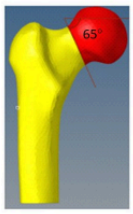


Figure 1 (A)

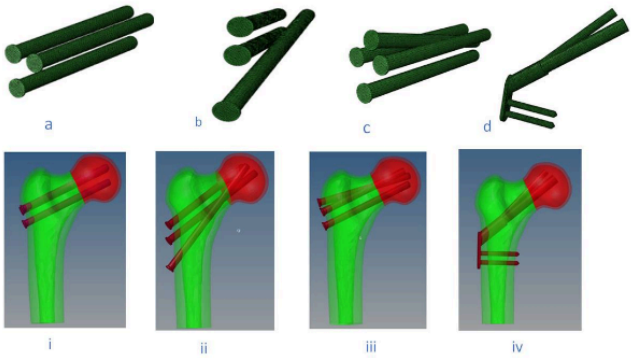


Figure 1 (B)

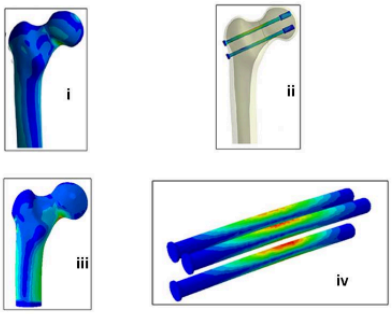


Figure 1 (C)

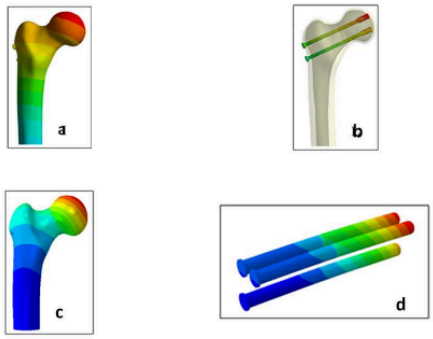


Figure 1 (D)

Figure 1

A: FE models of fracture neck fracture with Pauwels type III (65 °)

B: CAD of various CCS configuration, a,i:3-CCS; b,ii: BDSF; c,iii: 4-CCS, d,iv: FNS

C: Stress distribution of bone & implant in model by Li et al22 (i, ii) and our model (iii,iv)

D: Displacement distribution of bone & implant in model by Li et al22 (a,b) and our model (c,d)

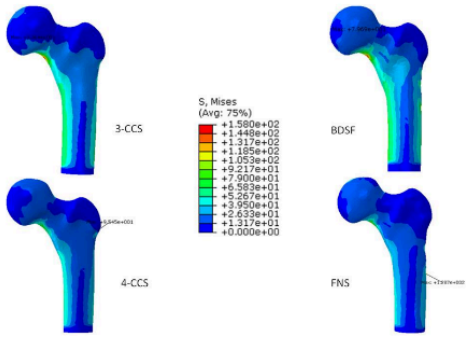


Figure 2 (A)

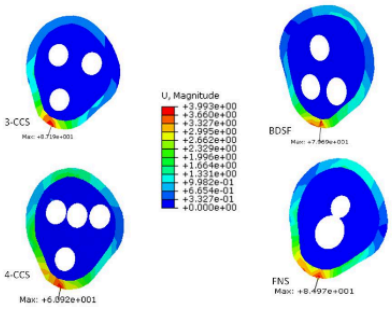


Figure 2 (B)

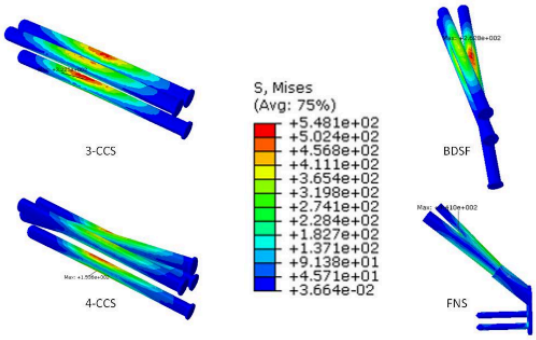


Figure 2 (C)

Figure 2

A: Von-Mises stress distribution of femur bone

B: Von-Mises stress distribution on Fracture surface

C: Von-Mises stress distribution of implant

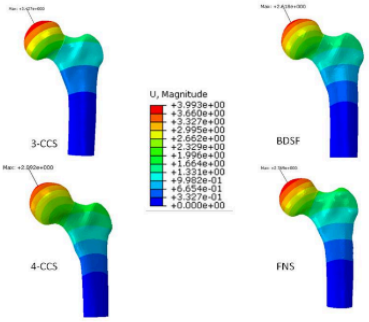


Figure 3 (A)

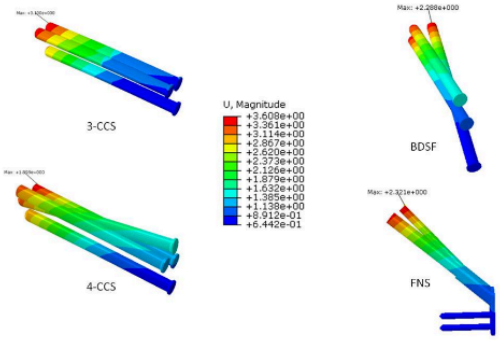


Figure 3 (B)

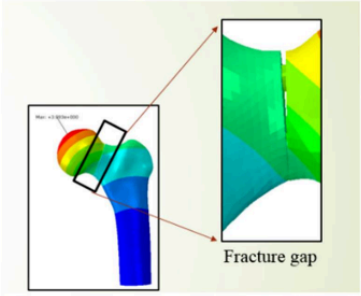


Figure 3 (C)

Figure 3

A: Displacement Distribution in Bone

B: Displacement Distribution in Implant

C: Maximum inter-fragmentary displacement (MIFD) of nodes at fracture gap

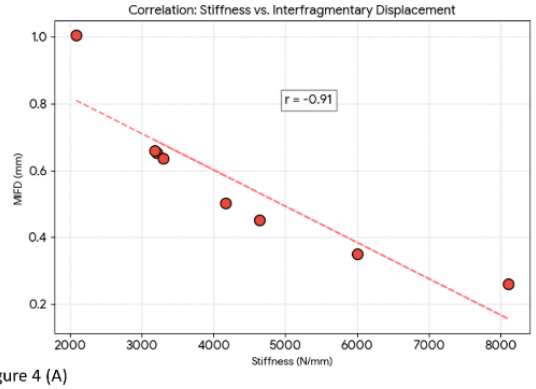


Figure 4 (A)

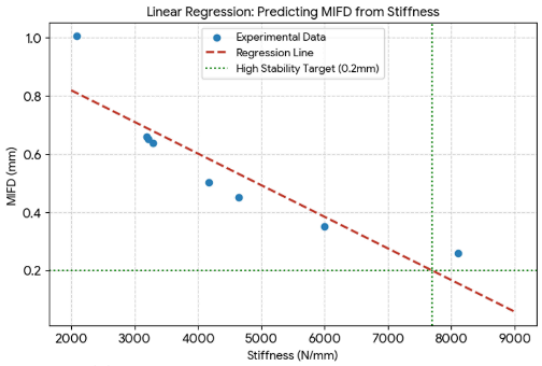


Figure 4 (B)

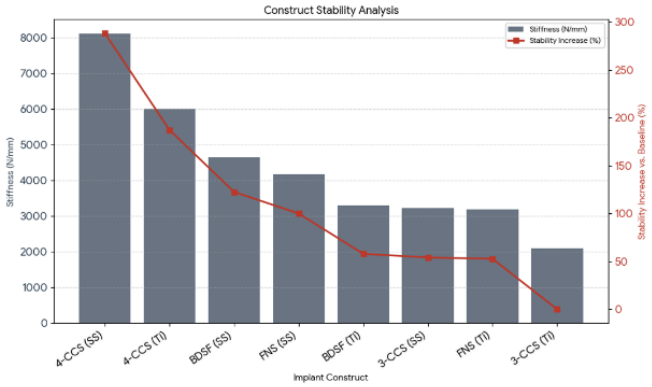


Figure 4 (C)

Figure 4

A: Correlation between Stiffness and Interfragmentary Displacement presented as a scatter plot showing the strong negative correlation (r = -0.91) between construct rigidity and fracture gap movement.

B: Linear Regression Model for Predicting MIFD; A visualization of the predictive equation MIFD =1.0369-(0.0001088 x Stiffness). The regression line indicates the theoretical stiffness required to meet specific clinical stability targets.

C: Construct Stiffness and Percentage Increase in Stability; A dual-axis chart showing absolute stiffness (N/mm) alongside the relative stability gain compared to the 3-CCS (Ti) baseline. The 4-CCS (SS) construct shows a peak stability increase of 288%.